

# *Rag2*<sup>-/-</sup> accelerates lipofuscin accumulation in the brain: Implications for human stem cell brain transplantation studies

Mengmeng Jin,<sup>1</sup> Mahabub Maraj Alam,<sup>1</sup> Alice Y.-C. Liu,<sup>1</sup> and Peng Jiang<sup>1,\*</sup>

<sup>1</sup>Department of Cell Biology and Neuroscience, Rutgers University, 604 Allison Road, Piscataway, NJ 08854, USA

\*Correspondence: [peng.jiang@rutgers.edu](mailto:peng.jiang@rutgers.edu)

<https://doi.org/10.1016/j.stemcr.2022.09.012>

## SUMMARY

Immunodeficient mice are widely used in human stem cell transplantation research. Recombination activating gene 1 (*Rag1*) deletion results in immunodeficiency and leads to accelerated aging in zebrafish with increased cytosolic accumulation of lipofuscin (LF). Unlike zebrafish, mammals have two homologs, *Rag1* and *Rag2*, that regulate adaptive immunity. Currently, little is known if and how *Rag1*<sup>-/-</sup> and *Rag2*<sup>-/-</sup> may impact aging and LF accumulation in immunodeficient mouse brains and how this may confound results in human neural cell transplantation studies. Here, we demonstrate that in *Rag2*<sup>-/-</sup> mouse brains, LF appears early, spreads broadly, emits strong autofluorescence, and accumulates with age. LF is found in various types of glial cells, including xenografted human microglia. Surprisingly, in *Rag1*<sup>-/-</sup> mouse brains, LF autofluorescence is seen at much older ages compared with *Rag2*<sup>-/-</sup> brains. This study provides direct evidence that *Rag2*<sup>-/-</sup> expedites LF occurrence and sets a context for studies using aged immunodeficient mice.

## INTRODUCTION

Transplantation of stem cells or progenitor cells of human origins into mice provides an exciting opportunity where the development of specific cells and their contribution to disease conditions can be studied under *in vivo* conditions (Jiang and Alam, 2022). Immunodeficient mice are widely used for transplantation of human cells without concerns of host immune rejections. Particularly, in the human stem cell and neuroscience research fields, immunodeficient mice have long been used as recipients for transplantation of human neural cells and developing human-mouse glial chimeric brain models (Windrem et al., 2004, 2008; Zhang et al., 2001). In recent years, with the development of human induced pluripotent stem cell technologies, immunodeficient mice lacking recombination-activating genes 1 or 2 (*Rag1* or *Rag2*) have been used to create microglial, macroglial (astroglia + oligodendroglia), and neuronal human-mouse brain chimeras (Chen et al., 2016; Espuny-Camacho et al., 2013, 2017; Han et al., 2013; Hasselmann et al., 2019; Linaro et al., 2019; Mancuso et al., 2019; Svoboda et al., 2019; Windrem et al., 2008; Xu et al., 2019, 2020), providing a platform to study the development and function of human neural cells *in vivo* under normal and diseased conditions.

Interestingly, a recent report in zebrafish showed that *Rag1* deletion leads to accelerated aging (Novoa et al., 2019). Zebrafish lacking *Rag1* showed an upregulation of genes associated with inflammation and a downregulation of genes involved in DNA damage and repair (Novoa et al., 2019). These immunocompromised fish also showed an increased rate of senescence and an increased cytosolic accumulation of lipofuscin (LF) (Novoa et al., 2019), one of the most consistent features of aging. LF is a complex

macromolecule, which is an amalgamate of various cellular metabolites of distinct origins (Hohn and Grune, 2013; Snyder and Crane, 2022). The degree of LF accumulation has been shown to correlate with aging (Singh Kushwaha et al., 2018). The composition of LF varies depending on the stage of aging, with a varying degree of oxidized proteins and sugar molecules being present (Benavides et al., 2002). It is well known that in postmitotic cells, such as neurons, LF accumulates over their lifespan (Jung et al., 2007; Liu et al., 2016). Furthermore, LF has been shown to accumulate in microglia, the resident macrophages of the brain (Xu et al., 2008), and cells of the macroglial lineage—astrocytes and oligodendrocytes (Uranova et al., 2018; Zalfa et al., 2016). Collectively, these observations suggest that *Rag1* may play a role in cellular senescence and accumulation of LF within the brain in zebrafish. While it has been reported that mice lacking *Rag1* or *Rag2* are susceptible to infections (Izadjoo et al., 2000; Wu et al., 2010), the accumulation of this well-known marker of aging, LF, in immunocompromised mice has not been reported.

In this study, we show that *Rag2*<sup>-/-</sup> mice across multiple genetic backgrounds share the common phenotype of a premature and age-dependent accumulation of LF, starting from 5 to 6 months old. Unexpectedly, the levels of LF detected in *Rag1*<sup>-/-</sup> mice are minimal compared with *Rag2*<sup>-/-</sup> mice at the comparable chronological age of 5 months. Thus, although *Rag1* and *Rag2* serve similar functions in the development of the immune system as a form of V(D)J recombination, we find that *Rag1*<sup>-/-</sup> and *Rag2*<sup>-/-</sup> have different impacts on the accumulation of LF, suggesting that *Rag1* and *Rag2* may play differential roles in aging of the mammalian brain. Importantly, our findings have critical implications for studies involving human stem cell



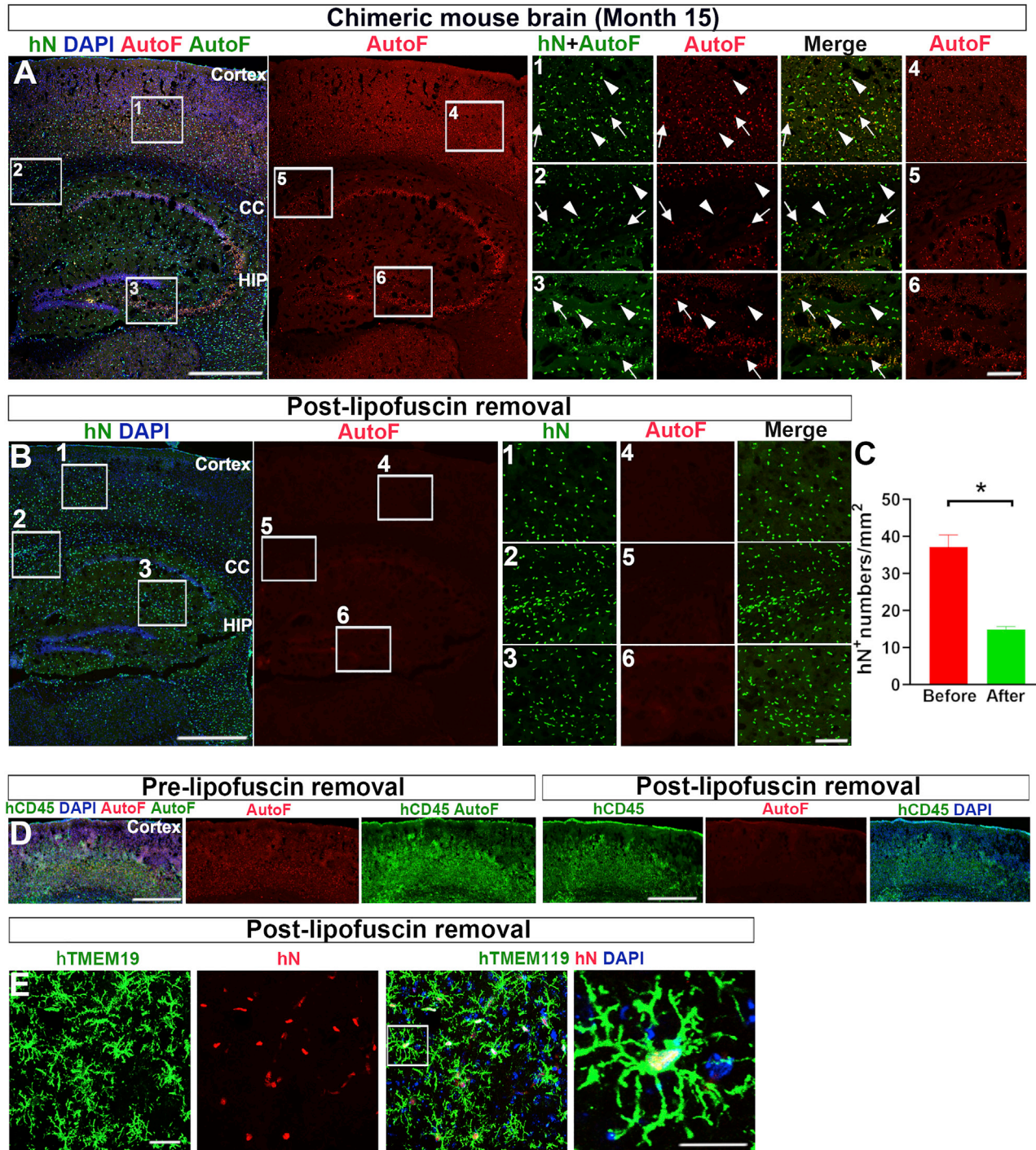


**Figure 1. Confounding results in chimeric mouse brains**

(A and B) Representative images from sagittal brain sections show the distribution of AutoF and transplanted control hiPSC-derived microglia (hN<sup>+</sup>) at 15 months before and after LF removal. Arrowheads indicate hN<sup>+</sup> cells. Arrows indicate AutoF. Scale bars: 500 and 200  $\mu$ m in the original and enlarged images, respectively.

(C) Quantification of the number of hN<sup>+</sup> per mm<sup>2</sup> before and after LF removal (n = 3 mice per group). Student's t test. \*p < 0.05. Data are presented as mean  $\pm$  SEM.

(legend continued on next page)



transplantation into mouse brains regarding the selection of an appropriate immunodeficient mouse strain as the transplant recipient and the necessity of removing LF autofluorescent aggregates to avoid any potential misinterpretation of results.

## RESULTS

### Confounding results in human cell transplantation studies using aged immunodeficient mice

We have previously created human microglial mouse chimeras by transplanting human induced pluripotent stem cell (hiPSC)-derived primitive macrophage progenitors into the brains of postnatal day 0 (P0)  $Rag2^{-/-} IL2r\gamma^{-/-}$  hCSF1<sup>KI</sup> immunodeficient mice (Xu et al., 2020). In our recent studies (Jin et al., 2022; Xu et al., 2020), we mainly characterized the donor-derived human microglia in chimeric brains at ages of less than 6 months old. In this study, we further examined the distribution of transplanted human microglia in 15-month-old chimeric mice by staining human nuclei (hN) with a specific anti-hN antibody. Numerous hN<sup>+</sup> cells were found widely dispersed in the cerebral cortex, the corpus callosum (CC), and the hippocampus (HIP) (Figure 1A). Surprisingly, we observed strong and unknown autofluorescence (AutoF) under the red fluorescent channel—despite not using any red fluorescent antibody—with a pattern resembling the green-stained hN. This red AutoF also exhibited AutoF under the green channel (Figure 1A, arrows). On the other hand, at least some of the hN<sup>+</sup> green dots were not fluorescent in the red channel, suggesting that these were the bona fide donor-derived human cells (Figure 1A, arrowheads). The similarity in the AutoF and hN<sup>+</sup> staining pattern and the dual emission of the AutoF entity in both the red and green channels challenged our ability to quantitate the number and percentage of the transplanted hN<sup>+</sup> human cells in the mouse brain. Given the age of the animals, the intensity of AutoF, and existing literature background, we reasoned that this AutoF is likely attributable to LF.

Previous studies involving aged mice successfully removed LF for downstream immunohistochemical analyses (Chen et al., 2020). Thus, we treated the brain sections from 15-month-old chimeric mice by using TrueBlack LF AutoF Quencher (Biotium). Indeed, this treatment effectively removed all the AutoF signal and allowed for the correct determination of the number of hN<sup>+</sup> cells, which was 2- to 3-fold lower than that without removing LF from

the brain tissue (Figure 1C). Similarly, as shown in Figure 1D, the AutoF also interfered with the staining of human-specific CD45 (hCD45) in the cerebral cortex, an epitope expressed in all nucleated hematopoietic cells (Carson et al., 1998) and which we used to label donor-derived human microglia in the chimeric mouse brain. After LF removal treatment, the human microglia, labeled by hN and human-specific TMEM119 (hTMEM119) (Bennett et al., 2016), clearly exhibited ramified morphology in 6-month-old chimeric mouse brains (Figure 1E). Altogether, these results showed that the strong AutoF signal in aged  $Rag2^{-/-} IL2r\gamma^{-/-}$  hCSF1<sup>KI</sup> mice confound immunohistochemical analysis of transplanted human cells in the chimeric mouse brain.

### LF starts to accumulate at earlier ages in $Rag2^{-/-}$ mice than in $Rag1^{-/-}$ mice

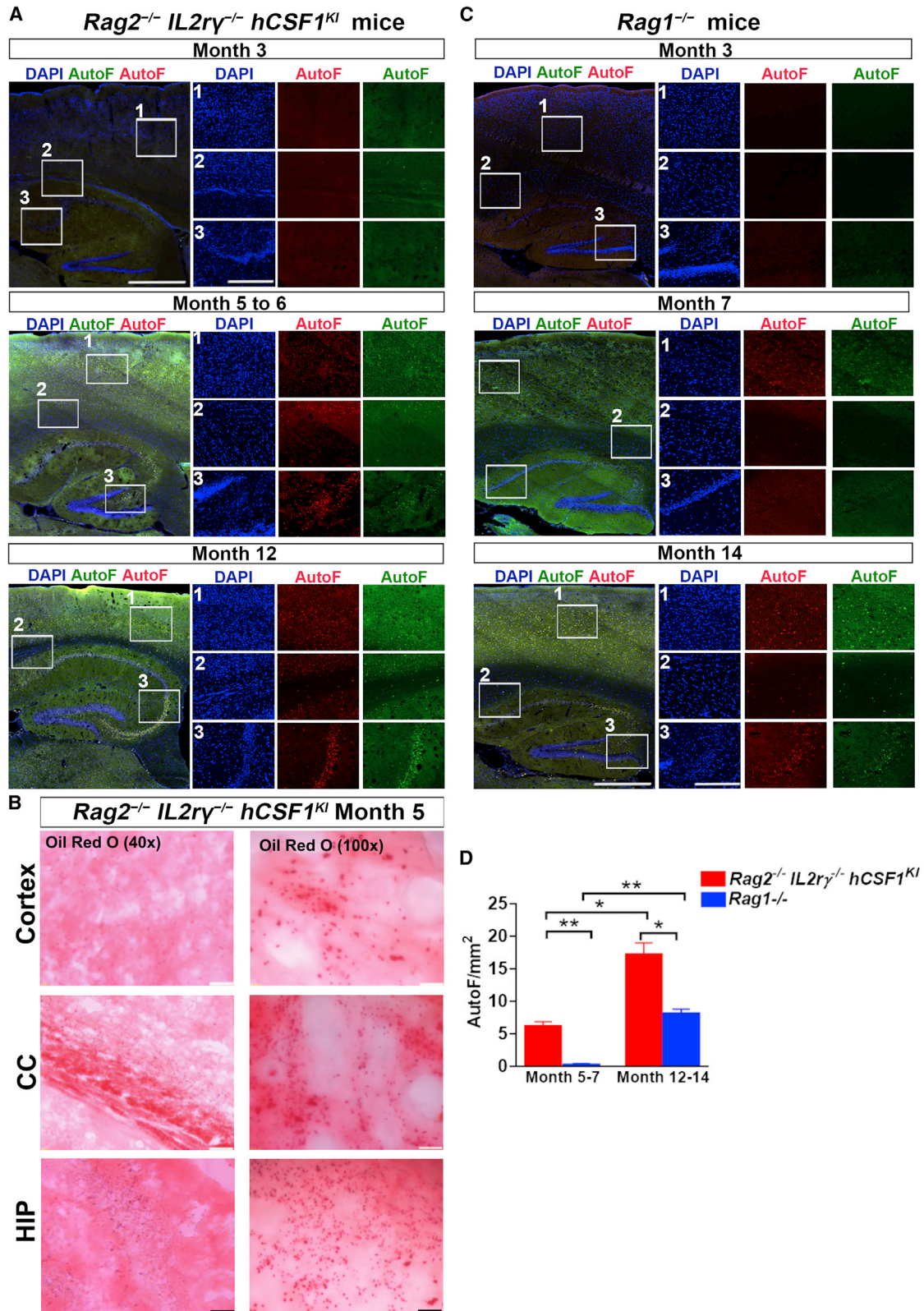
To characterize the temporal accumulation of AutoF in  $Rag2^{-/-} IL2r\gamma^{-/-}$  hCSF1<sup>KI</sup> mice, we examined the brains collected from 3- to 12-month-old mice. There was no AutoF in 3-month-old brains. Significant AutoF was first observed in the brains at 5–6 months of age (Figures 2A and 2D). The AutoF signal increased with age and was widely distributed in 12-month-old brains (Figure 2A). In addition, the identity of the AutoF was further affirmed to be LF by staining with oil red O, a widely used method for staining LF (Figure 2B). We further examined the accumulation of LF in  $Rag1^{-/-}$  mice. Interestingly, there was no AutoF in 3- to 7-month-old brains in  $Rag1^{-/-}$  mice (Figure 2C). Weak AutoF was first seen only in the cerebral cortex at around 7-month-old brains and became significant and broadly spread at the age of 14 months (Figure 2C). Interestingly, in 7-month-old  $Rag2^{-/-}$  mice on the same genetic background as the  $Rag1^{-/-}$  mice (C57BL/6), very strong and broadly spread AutoF had already been seen (Figure S1A). Taken together, we find that LF accumulates earlier in  $Rag2^{-/-}$  than in  $Rag1^{-/-}$  mice.

### Early accumulation of LF is consistently seen in $Rag2^{-/-}$ mice across different genetic backgrounds

To explore whether the accumulation of LF in  $Rag2^{-/-} IL2r\gamma^{-/-}$  hCSF1<sup>KI</sup> mice was caused by this particular genetic background and/or the additional knockout and knockin genetic modifications, we further examined the brains of two different  $Rag2^{-/-}$  mouse strains:  $Rag2^{-/-}$  mice on BALB/c genetic background and shiverer (*shi/shi*) ×  $Rag2^{-/-}$  mice on C3H background (Table S1). Consistently, as early as 5 months of age, we observed significant AutoF in both

(D) Representative images from sagittal brain sections show the distribution of AutoF and transplanted control hiPSC-derived microglia (hCD45<sup>+</sup>) in the cortex at 15 months. Scale bars: 500 and 200  $\mu$ m in the original and enlarged images, respectively.

(E) Representative images of human microglia (hTMEM119<sup>+</sup>/hN<sup>+</sup>) in 6-month-old chimeras after LF removal. The squared area is enlarged. Scale bars: 20 and 10  $\mu$ m in the original and enlarged images, respectively.



(legend on next page)



*Rag2*<sup>-/-</sup> and *shi/shi* × *Rag2*<sup>-/-</sup> mice (Figures 3A and 3B). Although in *shi/shi* × *Rag2*<sup>-/-</sup> mouse brains, the AutoF appeared to be weaker than that in *Rag2*<sup>-/-</sup> mouse brains, the presence of LF was nonetheless confirmed by the oil red O staining (Figure 3C). Furthermore, we integrated quantification of AutoF levels in *Rag2*<sup>-/-</sup> *IL2rγ*<sup>-/-</sup> *hCSF1*<sup>KI</sup> (BALB/c), *Rag1*<sup>-/-</sup> (C57BL/6), *Rag2*<sup>-/-</sup> (BALB/c), and *shi/shi* × *Rag2*<sup>-/-</sup> (C3H) mice. The results indicated that all three *Rag2*<sup>-/-</sup> strains showed accelerated LF accumulation compared with the *Rag1*<sup>-/-</sup> strain. In addition, we examined the baseline mouse strains, including C57BL/6, BALB/c, and C3H mice at the ages of 7 months. We found no AutoF in all of these mice (Figures S1B–S1D). Altogether, our data indicate that the early occurrence of LF in *Rag2*<sup>-/-</sup> mice is independent of their genetic background.

### LF accumulates in both human and mouse glial cells in the human microglial chimeric mouse brains

It is well known that LF accumulates in aged neurons (Gillis et al., 2016). In this study, we observed that LF appeared in different sizes in different brain regions, particularly in the white matter. Here, we thus focused on the accumulation of LF in glial cells in human-mouse chimeric brains. We found that LF accumulated in Iba1<sup>+</sup> microglial cells (Figure 4A), in GFAP<sup>+</sup> astrocytes (Figure 4B), and in CNPase<sup>+</sup> oligodendrocytes (Figure 4C). Since our chimeric mouse contained donor-derived human microglia, we asked if LF accumulation is also seen in xenografted human microglia. As shown in Figure 4D, LF accumulation was indeed found within xenografted microglia labeled by hTMEM119 antibody. Taken together, these results demonstrate that LF is distributed widely and prematurely in host mouse glial cells as well as in xenografted human microglial cells in the *Rag2*<sup>-/-</sup> *IL2rγ*<sup>-/-</sup> *hCSF1*<sup>KI</sup> chimeric mouse brains.

## DISCUSSION

It is not surprising to observe accelerated accumulation of LF in *Rag2*<sup>-/-</sup> mice, as immunodeficiency has been linked to accelerated aging (Appay and Rowland-Jones, 2002; Singh Kushwaha et al., 2018), and the accumulation of LF is a well-known index of aging. However, it is unexpected

that *Rag1*<sup>-/-</sup> mice do not exhibit the premature LF aggregations phenotype as the *Rag2*<sup>-/-</sup> mice at comparable chronological ages. Direct evidence in zebrafish shows that zebrafish lacking *Rag1* exhibit accelerated aging and a higher LF accumulation compared with control zebrafish (Mittelbrunn and Kroemer, 2021; Novoa et al., 2019). One of the plausible explanations is that there is an enhanced need for upregulation of innate immunity due to a lack of adaptive immunity, which leads to an upregulation of inflammation and radical oxygen species, promoting senescence and aging (Novoa et al., 2019). Zebrafish only has *Rag1*, which regulates adaptive immunity, whereas mammals, including rodents and humans, possess two such genes: *Rag1* and *Rag2*. *Rag1*<sup>-/-</sup> and *Rag2*<sup>-/-</sup> mice are both considered immunodeficient. The fact that the early LF accumulation is only observed in the brains of multiple *Rag2*<sup>-/-</sup> mouse strains suggests that early LF accumulation in *Rag2*<sup>-/-</sup> mice may not solely result from immunodeficiency. *Rag1* and *Rag2* in the brain do show differential functions. *Rag1* is expressed in the HIP, and *Rag1*<sup>-/-</sup> mice show impaired social recognition memory, suggesting that *Rag1* plays a role in cognitive functions (McGowan et al., 2011). On the other hand, *Rag2*<sup>-/-</sup> mice do not show such memory loss (McGowan et al., 2011). *Rag2*, but not *Rag1*, is required for axonal growth and retinal ganglionic cell development, whereas *Rag1* is thought to be more involved in specifying neuronal identity (Alvarez-Lindo et al., 2019; Feng et al., 2005). Another study has demonstrated that *Rag2*<sup>-/-</sup> mice harboring SOD1 mutation show a remarkably shorter life span compared with their littermate control animals with SOD mutation only (Beers et al., 2008), which supports the idea that *Rag2* may have yet-to-be-uncovered novel, neuroprotective functions in the brain. It would be interesting and significant in future studies to identify the *Rag2*-specific, aging-related functions in the brain independent of its role in adaptive immunity.

Our findings have important implications for the studies involving the use of aged *Rag2*<sup>-/-</sup> mice. For instance, two studies published in 2015–2016 aimed to examine the role of the adaptive immune system in the beta-amyloid (Aβ) pathology of Alzheimer's disease but drew completely opposite conclusions (Marsh et al., 2016; Spani et al., 2015). Both studies used Alzheimer's disease (AD) mouse models that

### Figure 2. LF accumulates earlier in *Rag2*<sup>-/-</sup> *IL2rγ*<sup>-/-</sup> *hCSF1*<sup>KI</sup> mice than *Rag1*<sup>-/-</sup> mice

- (A) Representative images from sagittal brain sections show AutoF distribution at 3, 5–6, and 12 months of *Rag2*<sup>-/-</sup> *IL2rγ*<sup>-/-</sup> *hCSF1*<sup>KI</sup> mice. Scale bars: 500 and 200 μm in the original and enlarged images, respectively.
- (B) Bright-field micrographs show oil red O<sup>+</sup> staining in the cerebral cortex, corpus callosum (CC), and hippocampus (HIP) of *Rag2*<sup>-/-</sup> *IL2rγ*<sup>-/-</sup> *hCSF1*<sup>KI</sup> mice. Scale bars: 50 and 10 μm in the original (left) and enlarged images (right), respectively.
- (C) Representative images from sagittal brain sections show AutoF distribution at 3, 7, and 14 months of *Rag1*<sup>-/-</sup> mice. Scale bars: 500 and 200 μm in the original and enlarged images, respectively.
- (D) Quantification of AutoF intensity per mm<sup>2</sup> at different time points of *Rag2*<sup>-/-</sup> *IL2rγ*<sup>-/-</sup> *hCSF1*<sup>KI</sup> and *Rag1*<sup>-/-</sup> mice (n = 3 mice per group). One-way ANOVA test. \*p < 0.05, \*\*p < 0.01. Data are presented as mean ± SEM.

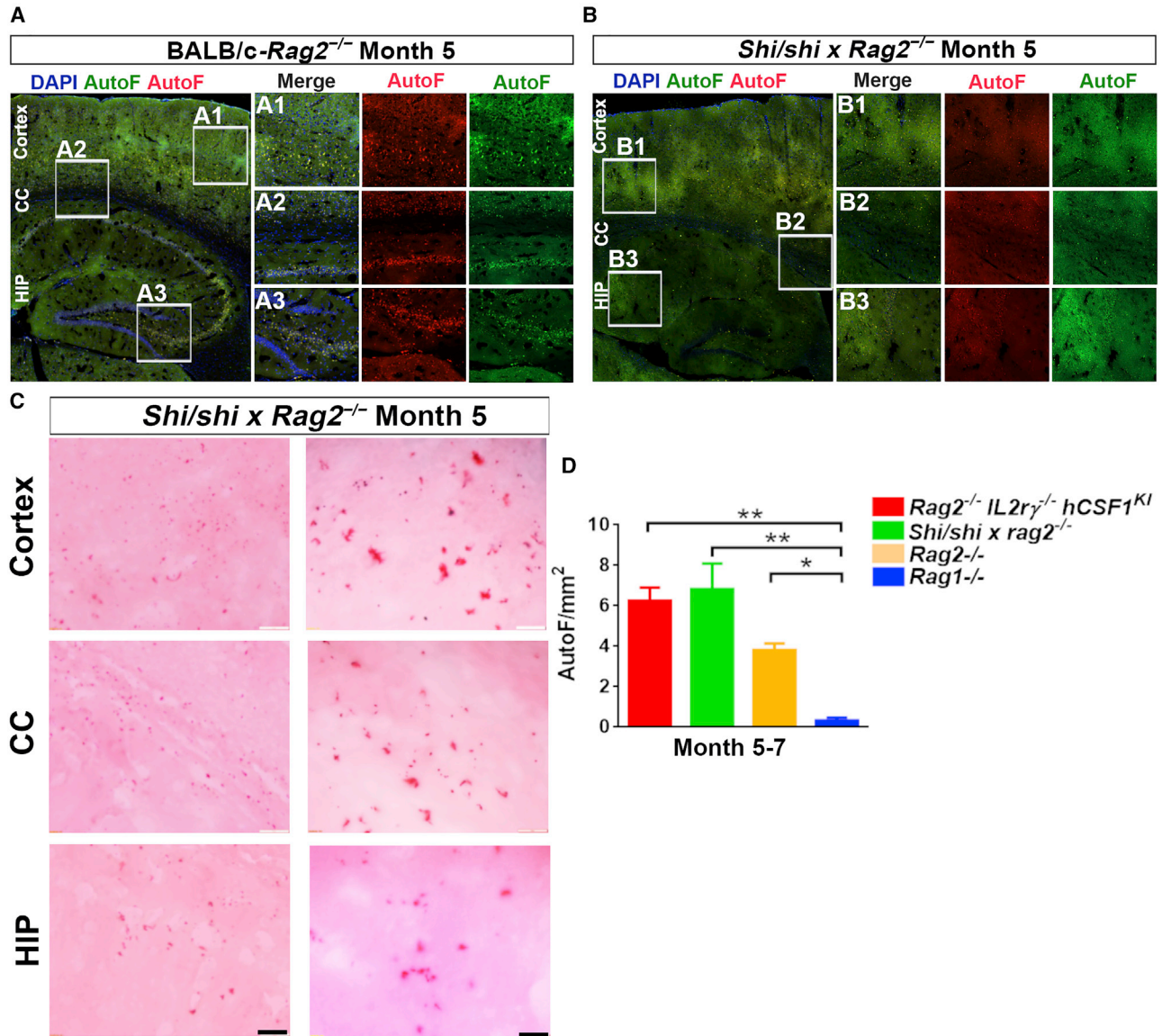


**Figure 3. LF accumulates in *Rag2*<sup>-/-</sup> mice across different genetic backgrounds**

(A and B) Representative images from sagittal brain sections showing the distribution of AutoF at 5 months of age in *Rag2*<sup>-/-</sup> *IL2rγ*<sup>-/-</sup> *hCSF1*<sup>KI</sup> and *shi/shi* × *Rag2*<sup>-/-</sup> mice. Scale bars: 500 and 200 μm in the original and enlarged images, respectively.

(C) Bright-field micrographs show oil red O<sup>+</sup> staining in the cortex, HIP, and CC of *shi/shi* × *Rag2*<sup>-/-</sup> mice. Scale bars: 50 and 10 μm in the original (left) and enlarged images (right), respectively.

(D) Quantification of AutoF intensity per mm<sup>2</sup> at different time points of *Rag2*<sup>-/-</sup> *IL2rγ*<sup>-/-</sup> *hCSF1*<sup>KI</sup> and *Rag1*<sup>-/-</sup> mice, as well as *Rag2*<sup>-/-</sup> (BALB/c) and *shi/shi* × *Rag2*<sup>-/-</sup> (C3H) (n = 3 mice per group). One-way ANOVA test. \*p < 0.05, \*\*p < 0.01, \*\*\*p < 0.001. Data are presented as mean ± SEM.

were crossed with immunodeficient *Rag2*<sup>-/-</sup> mice to generate AD mouse models lacking the adaptive immune system. Marsh et al. showed that immunodeficient AD mice exhibited greater Aβ pathology compared with immunocompetent AD mice with functional immune systems, suggesting that adaptive immune cell populations help restrain Aβ pathology (Marsh et al., 2016). On the other

hand, Späni et al. showed that Aβ pathology was greatly reduced in immunodeficient AD mice lacking functional adaptive immune cells (Späni et al., 2015). What could explain the discrepancy? Both studies used *Rag2*<sup>-/-</sup> mice of comparable chronological age (7–12 months). Perhaps some of the puncta-like “Aβ plaques” in these studies could have indeed been LF aggregates that were misinterpreted as

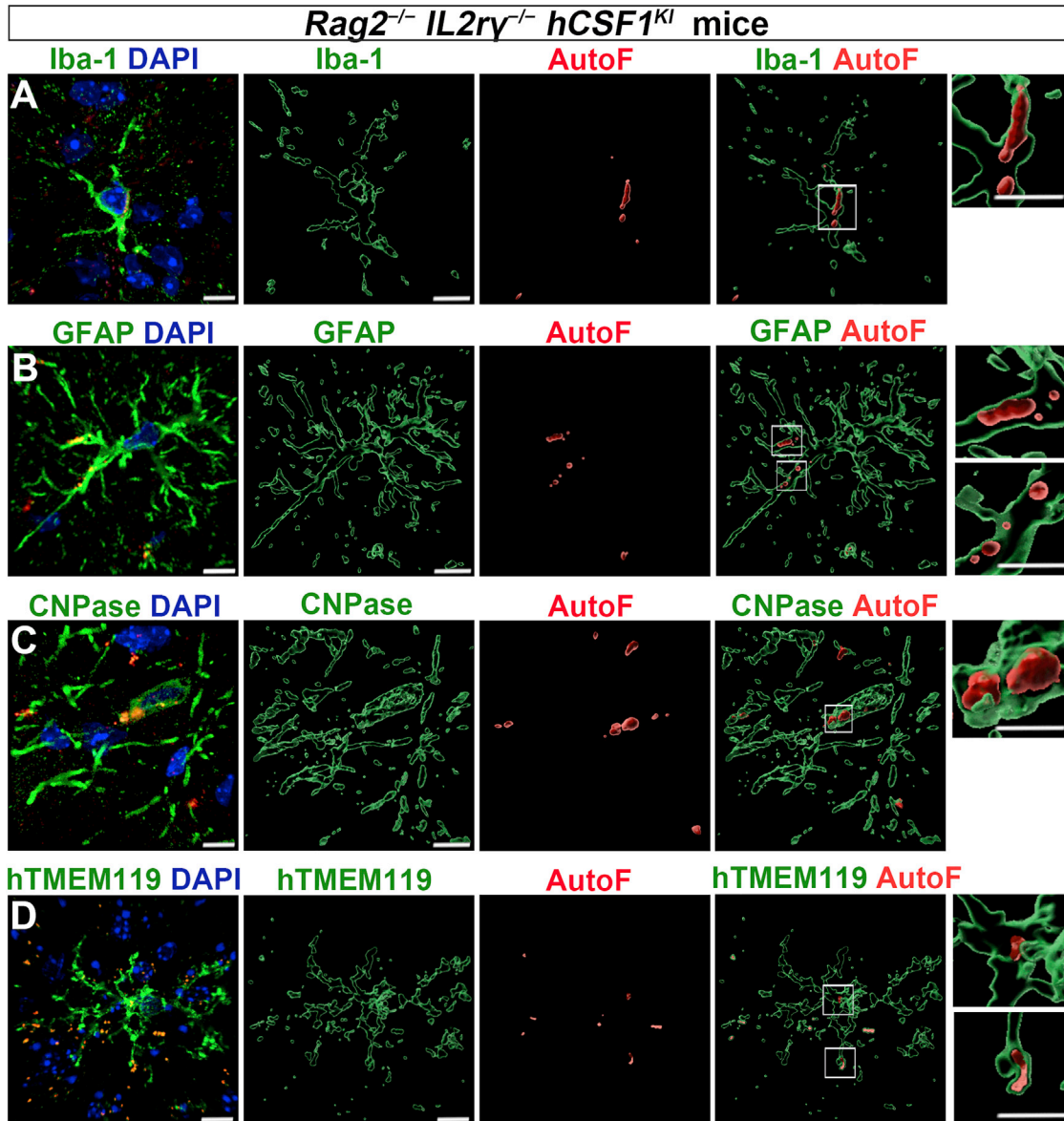


**Figure 4. LF accumulates in both host and transplanted glial cells in  $Rag2^{-/-} IL2ry^{-/-} hCSF1^{KI}$  mouse brains**

Representative raw fluorescent super-resolution and 3D surface rendered images showing Iba-1<sup>+</sup> staining (A), GFAP<sup>+</sup> staining (B), CNPase<sup>+</sup> staining (C), and human-specific TMEM119<sup>+</sup> (hTMEM119) staining (D) in 5- to 6-month-old  $Rag2^{-/-} IL2ry^{-/-} hCSF1^{KI}$  mice. Scale bars: 5 and 3  $\mu$ m in the original and enlarged images, respectively.

A $\beta$  plaques, since there is no information in the studies regarding whether LF removal treatment was performed. As both A $\beta$  plaques and LF do not have a generic stereotypical morphology, it can be difficult to determine from immunostaining data alone what staining signals are authentic A $\beta$  and what may be attributable to LF AutoF. It is noteworthy that LF AutoF has wide excitation (360–647 nm) and emission (500–640 nm) ranges of wavelength (Cho and Hwang, 2011), and LF aggregates can appear as both green and red under the microscope (Haralampus-Grynawski et al.,

2003). In addition, the potential  $Rag2$ -specific neuroprotective function in the brain cannot be neglected. Taken together, due to AutoF of LF having very broad excitation and emission spectra, for immunohistochemical analyses in old  $Rag2^{-/-}$  mouse brains (i.e., >6 months), precautions must be taken, and LF removal should be performed, particularly when examining proteins with puncta-like immunostaining patterns, such as synaptic markers, e.g., synapsin-1, PSD95, etc., and protein aggregates, e.g., soluble A $\beta$ , soluble hyperphosphorylated tau, etc.



Immunodeficient mice are widely used for stem cell transplantation studies. Our current findings also provide useful guidance regarding the selection of appropriate immunodeficient mouse strains as transplant recipients of human neural cells. Recently, we developed a chimeric mouse model by transplanting hiPSC-derived microglia into the brain of neonatal *Rag2*<sup>-/-</sup> *IL2r $\gamma$* <sup>-/-</sup> hCSF1<sup>KI</sup> mice (Xu et al., 2020). The engrafted hiPSC-derived microglia proliferate, migrate, and widely disperse in the adult mouse brain. At 6 months post-transplantation, xenografted hiPSC-derived microglia recapitulate features of adult human microglia at the transcriptomic and functional levels (Xu et al., 2020). We think that maturation of donor-derived human microglia is accelerated in the much faster-developing mouse brain relative to the human brain, particularly in the *Rag2*<sup>-/-</sup> mouse brains with accelerated aging. It is challenging to model aging-related neurodegenerative diseases with hiPSCs because hiPSC-derived neural cells grown in two-dimensional (2D) cultures or 3D organoid/spheroid cultures exhibit limited cellular maturation even after long-term culture, and they mostly approximate brain cells in prenatal or early postnatal stages (Di Lullo and Kriegstein, 2017; Patterson et al., 2012). Thus, engrafting those hiPSC-derived neural cells into the brains of *Rag2*<sup>-/-</sup> mouse strains may facilitate analysis of aging-dependent pathological changes in human neural cells. hiPSCs have also been generated from disorders that show accelerated aging, such as Down syndrome (Chen et al., 2014; Cuadrado and Barrena, 1996; Horvath et al., 2015; Lott and Head, 2005; Teipel and Hampel, 2006). In addition, a previous study demonstrates that hiPSC-derived neurons that express progerin, a truncated form of lamin A associated with premature aging, exhibit aging-related markers and characteristics (Miller et al., 2013). Transplantation of these and related hiPSC-derived neural cells with premature genetic makeup into the brains of *Rag2*<sup>-/-</sup> mice that confer a premature aging host environment would greatly facilitate analysis of the interplay of intrinsic/genetic versus extrinsic/environmental factors in driving age-related pathologies in neurodegenerative diseases. Our recent study showcasing Down syndrome microglia are prone to pathologic tau-associated senescence provides an example of such possibilities (Jin et al., 2022).

## EXPERIMENTAL PROCEDURES

### Animals

All animal work was performed without gender bias with the approval of the Rutgers University Institutional Animal Care and Use Committee. The animals used in this study are summarized in Table S1.

### hiPSC culture

One control hiPSC line was used in this study. The hiPSCs were cultured on dishes coated with hESC-qualified Matrigel (Corning) in mTeSR plus media (STEMCELL Technologies) under a feeder-free condition. The hiPSCs were passaged with ReLeSR media (STEMCELL Technologies) once per week.

### Differentiation and culture of PMPs

Primitive macrophage progenitors (PMPs) were generated from the control hiPSC cell line using a previously established protocol (Haenseler et al., 2017). The yolk sac embryoid bodies (YS-EBs) were generated by treating the YS-EBs with mTeSR 1 media (STEMCELL Technologies) supplemented with bone morphogenetic protein 4 (BMP4; 50 ng/mL), vascular endothelial growth factor (VEGF; 50 ng/mL), and stem cell factor (SCF; 20 ng/mL) for 6 days. To stimulate myeloid differentiation, the YS-EBs were plated on dishes with X-VIVO 15 medium (Lonza) supplemented with interleukin-3 (IL-3; 25 ng/mL) and macrophage colony-stimulating factor (M-CSF; 100 ng/mL). At 4–6 weeks after plating, human PMPs emerged into the supernatant and were continuously produced for more than 3 months.

### Cell transplantation

PMPs were collected from the supernatant and suspended at a concentration of 100,000 cells/ $\mu$ L in PBS. Cells were then injected into the brains of P0 *Rag2*<sup>-/-</sup> *IL2r $\gamma$* <sup>-/-</sup> hCSF1<sup>KI</sup> immunodeficient mice (C; 129S4-*Rag2*<sup>tm1.1Flv</sup> *Csf1tm1*<sup>(CSF1)Flv</sup> *Il2rg*<sup>tm1.1Flv</sup>/J, The Jackson Laboratory; stock no. 017708). The transplantation sites were bilateral from the midline =  $\pm$ 1.0 mm, posterior from bregma = -2.0 mm, and dorsoventral depths = -1.5 and -1.2 mm (Xu et al., 2020). The pups were placed in ice for 4 to 5 min to anesthetize them and then injected with 0.5  $\mu$ L of cells into each site (four sites total) using a digital stereotaxic device (David KOPF Instruments) that was equipped with a neonatal mouse adapter (Stoelting).

### Tissue immunostaining, image acquisition, and analysis

Mouse brains were fixed with 4% paraformaldehyde. The brains were then placed in 20%, and later in 30%, sucrose for dehydration. Following dehydration, brain tissues were immersed in optimal cutting temperature (O.C.T) compound and frozen for sectioning. The frozen tissues were cryo-sectioned with 30  $\mu$ m thickness for immunofluorescence staining. The tissues were blocked with a blocking solution (5% goat serum in PBS with 0.8% Triton X-100) at room temperature (RT) for 1 h. The primary antibodies were diluted in the same blocking solution and incubated with the tissues at 4°C overnight (all the primary antibodies are listed in Table S1). The sections were washed with PBS and incubated with secondary antibodies for 1 h at RT. After washing with PBS, the slides were mounted with anti-fade Fluoromount-G medium containing DAPI (1, 40,6-diamidino-2-phenylindole dihydrochloride) (Southern Biotechnology).

All fluorescent images were captured with a Zeiss 800 confocal microscope. Large scale images in Figures 1A, 2A, 2B, 4A–4D, and S1A–S1D were obtained by confocal tile scan by the Zen software (Zeiss). To obtain a 3D reconstruction, images were processed by the Zen software (Zeiss).



For each animal, whole-brain tile images were taken from 3–5 brain sections and used for quantification. LF AutoF intensity under red channel was analyzed and quantified using ImageJ (NIH).

### Lipid staining

Stock solution of oil red O stain was prepared by dissolving 50 mg oil red O powder (Sigma; O-0625) in 10 mL isopropanol. A 37°C water bath was used to gently heat the solution to facilitate dissolution of the solid. Working solution of oil red O stain was prepared by diluting 3 mL of the stock solution with 2 mL distilled water for a total volume of 5 mL. The solution was then filtered. Working solution was prepared fresh each time. Frozen tissue sections were washed in PBS to remove OCT compound. Tissue sections were then immersed in 60% isopropanol for 30 s and stained with freshly prepared oil red O working solution for 15 min. Stained tissue sections were then immersed in 60% isopropanol for 30 s and mounted using mounting media. All the images were captured by a wide-field microscope (Olympus BX63).

### TrueBlack treatment

TrueBlack (1×) solution was prepared by diluting 50× TrueBlack (Biotium) stock solution in 70% ethanol, according to the manufacturer's instructions. The solution was vortexed to mix well and shielded from light. Following immunostaining, brain slices were removed from PBS. The sections were covered with 1× TrueBlack solution for 20 s. After that, the 1× TrueBlack solution was discarded, and the sections were rinsed three times with PBS.

### Statistical analysis

All data are represented as mean ± SEM. When only two independent groups were compared, significance was determined by using two-tailed unpaired t test with Welch's correction or paired t test. When three or more groups were compared, one-way ANOVA with Bonferroni post-hoc test was used. A p value of <0.05 was considered significant. All the analyses were done in GraphPad Prism v.9.

### SUPPLEMENTAL INFORMATION

Supplemental information can be found online at <https://doi.org/10.1016/j.stemcr.2022.09.012>.

### AUTHOR CONTRIBUTIONS

M.J. and P.J. designed experiments and interpreted data; M.J. carried out most experiments with technical assistance from M.M.A.; A.Y.-C.L. provided study materials and reagents and provided critical suggestions to the overall research direction. P.J. directed the project and wrote the manuscript together with M.J., M.M.A., and A.Y.-C.L.

### ACKNOWLEDGMENTS

This work was supported in part by grants from the NIH (R01NS102382, R01NS122108, and R01AG073779 to P.J.). M.M.A. is supported by the Rutgers PhD Training Program in Biotechnology funded by the NIH (T32 GM135141).

### CONFLICT OF INTERESTS

The authors declare no competing financial interests.

Received: June 2, 2022

Revised: September 23, 2022

Accepted: September 26, 2022

Published: October 20, 2022

### REFERENCES

- Alvarez-Lindo, N., Baleriola, J., de Los Rios, V., Suarez, T., and de la Rosa, E.J. (2019). RAG-2 deficiency results in fewer phosphorylated histone H2AX foci, but increased retinal ganglion cell death and altered axonal growth. *Sci. Rep.* *9*, 18486. <https://doi.org/10.1038/s41598-019-54873-w>.
- Appay, V., and Rowland-Jones, S.L. (2002). Premature ageing of the immune system: the cause of AIDS? *Trends Immunol.* *23*, 580–585. [https://doi.org/10.1016/s1471-4906\(02\)02338-4](https://doi.org/10.1016/s1471-4906(02)02338-4).
- Beers, D.R., Henkel, J.S., Zhao, W., Wang, J., and Appel, S.H. (2008). CD4+ T cells support glial neuroprotection, slow disease progression, and modify glial morphology in an animal model of inherited ALS. *Proc. Natl. Acad. Sci. USA* *105*, 15558–15563. <https://doi.org/10.1073/pnas.0807419105>.
- Benavides, S.H., Monserrat, A.J., Farina, S., and Porta, E.A. (2002). Sequential histochemical studies of neuronal lipofuscin in human cerebral cortex from the first to the ninth decade of life. *Arch. Gerontol. Geriatr.* *34*, 219–231. [https://doi.org/10.1016/s0167-4943\(01\)00223-0](https://doi.org/10.1016/s0167-4943(01)00223-0).
- Bennett, M.L., Bennett, F.C., Liddel, S.A., Ajami, B., Zamanian, J.L., Fernhoff, N.B., Mulinyawe, S.B., Bohlen, C.J., Adil, A., Tucker, A., et al. (2016). New tools for studying microglia in the mouse and human CNS. *Proc. Natl. Acad. Sci. USA* *113*, E1738–E1746. <https://doi.org/10.1073/pnas.1525528113>.
- Carson, M.J., Reilly, C.R., Sutcliffe, J.G., and Lo, D. (1998). Mature microglia resemble immature antigen-presenting cells. *Glia* *22*, 72–85. [https://doi.org/10.1002/\(sici\)1098-1136\(199801\)22:1<72::aid-glia7>3.0.co;2-a](https://doi.org/10.1002/(sici)1098-1136(199801)22:1<72::aid-glia7>3.0.co;2-a).
- Chen, C., Jiang, P., Xue, H., Peterson, S.E., Tran, H.T., McCann, A.E., Parast, M.M., Li, S., Pleasure, D.E., Laurent, L.C., et al. (2014). Role of astroglia in Down's syndrome revealed by patient-derived human-induced pluripotent stem cells. *Nat. Commun.* *5*, 4430. <https://doi.org/10.1038/ncomms5430>.
- Chen, C., Kim, W.Y., and Jiang, P. (2016). Humanized neuronal chimeric mouse brain generated by neonatally engrafted human iPSC-derived primitive neural progenitor cells. *JCI Insight* *1*, e88632. <https://doi.org/10.1172/jci.insight.88632>.
- Chen, W.T., Lu, A., Craessaerts, K., Pavie, B., Sala Frigerio, C., Corthout, N., Qian, X., Lalakova, J., Kuhnemund, M., Voytyuk, I., et al. (2020). Spatial transcriptomics and in situ sequencing to study Alzheimer's disease. *Cell* *182*, 976–991. <https://doi.org/10.1016/j.cell.2020.06.038>.
- Cho, S., and Hwang, E.S. (2011). Fluorescence-based detection and quantification of features of cellular senescence. *Methods Cell Biol.* *103*, 149–188. <https://doi.org/10.1016/b978-0-12-385493-3.00007-3>.



- Cuadrado, E., and Barrena, M.J. (1996). Immune dysfunction in Down's syndrome: primary immune deficiency or early senescence of the immune system? *Clin. Immunol. Immunopathol.* *78*, 209–214. <https://doi.org/10.1006/clin.1996.0031>.
- Di Lullo, E., and Kriegstein, A.R. (2017). The use of brain organoids to investigate neural development and disease. *Nat. Rev. Neurosci.* *18*, 573–584. <https://doi.org/10.1038/nrn.2017.107>.
- Espuny-Camacho, I., Arranz, A.M., Fiers, M., Snellinx, A., Ando, K., Munck, S., Bonnefont, J., Lambot, L., Corthout, N., Omodho, L., et al. (2017). Hallmarks of Alzheimer's disease in stem-cell-derived human neurons transplanted into mouse brain. *Neuron* *93*, 1066–1081.e8. <https://doi.org/10.1016/j.neuron.2017.02.001>.
- Espuny-Camacho, I., Michelsen, K.A., Gall, D., Linaro, D., Hasche, A., Bonnefont, J., Bali, C., Orduz, D., Bilheu, A., Herpoel, A., et al. (2013). Pyramidal neurons derived from human pluripotent stem cells integrate efficiently into mouse brain circuits in vivo. *Neuron* *77*, 440–456. <https://doi.org/10.1016/j.neuron.2012.12.011>.
- Feng, B., Bulchand, S., Yaksi, E., Friedrich, R.W., and Jesuthasan, S. (2005). The recombination activation gene 1 (Rag1) is expressed in a subset of zebrafish olfactory neurons but is not essential for axon targeting or amino acid detection. *BMC Neurosci.* *6*, 46. <https://doi.org/10.1186/1471-2202-6-46>.
- Gilissen, E.P., Leroy, K., Yilmaz, Z., Kovari, E., Bouras, C., Boom, A., Poncet, L., Erwin, J.M., Sherwood, C.C., Hof, P.R., and Brion, J.P. (2016). A neuronal aging pattern unique to humans and common chimpanzees. *Brain Struct. Funct.* *221*, 647–664. <https://doi.org/10.1007/s00429-014-0931-5>.
- Haenseler, W., Sansom, S.N., Buchrieser, J., Newey, S.E., Moore, C.S., Nicholls, F.J., Chintawar, S., Schnell, C., Antel, J.P., Allen, N.D., et al. (2017). A highly efficient human pluripotent stem cell microglia model displays a neuronal-Co-culture-Specific expression profile and inflammatory response. *Stem Cell Rep.* *8*, 1727–1742. <https://doi.org/10.1016/j.stemcr.2017.05.017>.
- Han, X., Chen, M., Wang, F., Windrem, M., Wang, S., Shanz, S., Xu, Q., Oberheim, N.A., Bekar, L., Betstadt, S., et al. (2013). Forebrain engraftment by human glial progenitor cells enhances synaptic plasticity and learning in adult mice. *Cell Stem Cell* *12*, 342–353. <https://doi.org/10.1016/j.stem.2012.12.015>.
- Haralampus-Grynaviski, N.M., Lamb, L.E., Clancy, C.M.R., Skumatz, C., Burke, J.M., Sarna, T., and Simon, J.D. (2003). Spectroscopic and morphological studies of human retinal lipofuscin granules. *Proc. Natl. Acad. Sci. USA* *100*, 3179–3184. <https://doi.org/10.1073/pnas.0630280100>.
- Hasselmann, J., Coburn, M.A., England, W., Figueroa Velez, D.X., Kiani Shabestari, S., Tu, C.H., McQuade, A., Kolahdouzan, M., Echeverria, K., Claes, C., et al. (2019). Development of a chimeric model to study and manipulate human microglia in vivo. *Neuron* *103*, 1016–1033.e10. <https://doi.org/10.1016/j.neuron.2019.07.002>.
- Hohn, A., and Grune, T. (2013). Lipofuscin: formation, effects and role of macroautophagy. *Redox Biol.* *1*, 140–144. <https://doi.org/10.1016/j.redox.2013.01.006>.
- Horvath, S., Garagnani, P., Bacalini, M.G., Pirazzini, C., Salvioi, S., Gentilini, D., Di Blasio, A.M., Giuliani, C., Tung, S., Vinters, H.V., and Franceschi, C. (2015). Accelerated epigenetic aging in Down syndrome. *Aging Cell* *14*, 491–495. <https://doi.org/10.1111/accel.12325>.
- Izadjoo, M.J., Polotsky, Y., Mense, M.G., Bhattacharjee, A.K., Paravitana, C.M., Hadfield, T.L., and Hoover, D.L. (2000). Impaired control of *Brucella melitensis* infection in Rag1-deficient mice. *Infect. Immun.* *68*, 5314–5320. <https://doi.org/10.1128/iai.68.9.5314-5320.2000>.
- Jiang, P., and Alam, M.M. (2022). Rise of the human-mouse chimeric brain models. *Cell Regen.* *11*, 32. <https://doi.org/10.1186/s13619-022-00135-6>.
- Jin, M., Xu, R., Wang, L., Alam, M.M., Ma, Z., Zhu, S., Martini, A.C., Jadali, A., Bernabucci, M., Xie, P., et al. (2022). Type-I-interferon signaling drives microglial dysfunction and senescence in human iPSC models of Down syndrome and Alzheimer's disease. *Cell Stem Cell* *29*, 1135–1153.e8. <https://doi.org/10.1016/j.stem.2022.06.007>.
- Jung, T., Bader, N., and Grune, T. (2007). Lipofuscin: formation, distribution, and metabolic consequences. *Ann. N. Y. Acad. Sci.* *1119*, 97–111. <https://doi.org/10.1196/annals.1404.008>.
- Linaro, D., Vermaercke, B., Iwata, R., Ramaswamy, A., Libe-Philipot, B., Boubakar, L., Davis, B.A., Wierda, K., Davie, K., Poovathingal, S., et al. (2019). Xenotransplanted human cortical neurons reveal species-specific development and functional integration into mouse visual circuits. *Neuron* *104*, 972–986.e6. <https://doi.org/10.1016/j.neuron.2019.10.002>.
- Liu, J.Y.W., Reeves, C., Diehl, B., Coppola, A., Al-Hajri, A., Hoskote, C., Mughairy, S.A., Tachrount, M., Groves, M., Michalak, Z., et al. (2016). Early lipofuscin accumulation in frontal lobe epilepsy. *Ann. Neurol.* *80*, 882–895. <https://doi.org/10.1002/ana.24803>.
- Lott, I.T., and Head, E. (2005). Alzheimer disease and Down syndrome: factors in pathogenesis. *Neurobiol. Aging* *26*, 383–389. <https://doi.org/10.1016/j.neurobiolaging.2004.08.005>.
- Mancuso, R., Van Den Daele, J., Fattorelli, N., Wolfs, L., Balusu, S., Burton, O., Liston, A., Sierksma, A., Fournie, Y., Poovathingal, S., et al. (2019). Stem-cell-derived human microglia transplanted in mouse brain to study human disease. *Nat. Neurosci.* *22*, 2111–2116. <https://doi.org/10.1038/s41593-019-0525-x>.
- Marsh, S.E., Abud, E.M., Lakatos, A., Karimzadeh, A., Yeung, S.T., Davtyan, H., Fote, G.M., Lau, L., Weinger, J.G., Lane, T.E., et al. (2016). The adaptive immune system restrains Alzheimer's disease pathogenesis by modulating microglial function. *Proc. Natl. Acad. Sci. USA* *113*, E1316–E1325. <https://doi.org/10.1073/pnas.1525466113>.
- McGowan, P.O., Hope, T.A., Meck, W.H., Kelsoe, G., and Williams, C.L. (2011). Impaired social recognition memory in recombination activating gene 1-deficient mice. *Brain Res.* *1383*, 187–195. <https://doi.org/10.1016/j.brainres.2011.02.054>.
- Miller, J.D., Ganat, Y.M., Kishinevsky, S., Bowman, R.L., Liu, B., Tu, E.Y., Mandal, P.K., Vera, E., Shim, J.W., Kriks, S., et al. (2013). Human iPSC-based modeling of late-onset disease via progerin-induced aging. *Cell Stem Cell* *13*, 691–705. <https://doi.org/10.1016/j.stem.2013.11.006>.
- Mittelbrunn, M., and Kroemer, G. (2021). Hallmarks of T cell aging. *Nat. Immunol.* *22*, 687–698. <https://doi.org/10.1038/s41590-021-00927-z>.



- Novoa, B., Pereiro, P., Lopez-Munoz, A., Varela, M., Forn-Cuni, G., Anchelín, M., Dios, S., Romero, A., Martínez-Lopez, A., Medina-Gali, R.M., et al. (2019). Rag1 immunodeficiency-induced early aging and senescence in zebrafish are dependent on chronic inflammation and oxidative stress. *Aging Cell* 18, e13020. <https://doi.org/10.1111/acer.13020>.
- Patterson, M., Chan, D.N., Ha, I., Case, D., Cui, Y., Handel, B.V., Mikkola, H.K., and Lowry, W.E. (2012). Defining the nature of human pluripotent stem cell progeny. *Cell Res.* 22, 178–193. <https://doi.org/10.1038/cr.2011.133>.
- Singh Kushwaha, S., Patro, N., and Kumar Patro, I. (2018). A sequential study of age-related lipofuscin accumulation in Hippocampus and striate cortex of rats. *Ann. Neurosci.* 25, 223–233. <https://doi.org/10.1159/000490908>.
- Snyder, A.N., and Crane, J.S. (2022). *Histology, Lipofuscin (StatPearls)*.
- Spani, C., Suter, T., Derungs, R., Ferretti, M.T., Welt, T., Wirth, F., Gericke, C., Nitsch, R.M., and Kulic, L. (2015). Reduced beta-amyloid pathology in an APP transgenic mouse model of Alzheimer's disease lacking functional B and T cells. *Acta neuropathol. Commun.* 3, 71. <https://doi.org/10.1186/s40478-015-0251-x>.
- Svoboda, D.S., Barrasa, M.I., Shu, J., Rietjens, R., Zhang, S., Mitalipova, M., Berube, P., Fu, D., Shultz, L.D., Bell, G.W., and Jaenisch, R. (2019). Human iPSC-derived microglia assume a primary microglia-like state after transplantation into the neonatal mouse brain. *Proc. Natl. Acad. Sci. USA* 116, 25293–25303. <https://doi.org/10.1073/pnas.1913541116>.
- Teipel, S.J., and Hampel, H. (2006). Neuroanatomy of Down syndrome in vivo: a model of preclinical Alzheimer's disease. *Behav. Genet.* 36, 405–415. <https://doi.org/10.1007/s10519-006-9047-x>.
- Uranova, N.A., Vikhрева, O.V., Rakhmanova, V.I., and Orlovskaya, D.D. (2018). Ultrastructural pathology of oligodendrocytes adjacent to microglia in prefrontal white matter in schizophrenia. *NPJ Schizophr* 4, 26. <https://doi.org/10.1038/s41537-018-0068-2>.
- Windrem, M.S., Nunes, M.C., Rashbaum, W.K., Schwartz, T.H., Goodman, R.A., McKhann, G., 2nd, Roy, N.S., and Goldman, S.A. (2004). Fetal and adult human oligodendrocyte progenitor cell isolates myelinate the congenitally dysmyelinated brain. *Nat. Med.* 10, 93–97. <https://doi.org/10.1038/nm974>.
- Windrem, M.S., Schanz, S.J., Guo, M., Tian, G.F., Washco, V., Stanwood, N., Rasband, M., Roy, N.S., Nedergaard, M., Havton, L.A., et al. (2008). Neonatal chimerization with human glial progenitor cells can both remyelinate and rescue the otherwise lethally hypomyelinated shiverer mouse. *Cell Stem Cell* 2, 553–565. <https://doi.org/10.1016/j.stem.2008.03.020>.
- Wu, H., Haist, V., Baumgartner, W., and Schughart, K. (2010). Sustained viral load and late death in Rag2<sup>-/-</sup> mice after influenza A virus infection. *Virology* 407, 172. <https://doi.org/10.1016/j.virus.2010.07.014>.
- Xu, H., Chen, M., Manivannan, A., Lois, N., and Forrester, J.V. (2008). Age-dependent accumulation of lipofuscin in perivascular and subretinal microglia in experimental mice. *Aging Cell* 7, 58–68. <https://doi.org/10.1111/j.1474-9726.2007.00351.x>.
- Xu, R., Brawner, A.T., Li, S., Liu, J.J., Kim, H., Xue, H., Pang, Z.P., Kim, W.Y., Hart, R.P., Liu, Y., and Jiang, P. (2019). OLIG2 drives abnormal neurodevelopmental phenotypes in human iPSC-based organoid and chimeric mouse models of Down syndrome. *Cell Stem Cell* 24, 908–926.e8. <https://doi.org/10.1016/j.stem.2019.04.014>.
- Xu, R., Li, X., Boreland, A.J., Posyton, A., Kwan, K., Hart, R.P., and Jiang, P. (2020). Human iPSC-derived mature microglia retain their identity and functionally integrate in the chimeric mouse brain. *Nat. Commun.* 11, 1577. <https://doi.org/10.1038/s41467-020-15411-9>.
- Zalfa, C., Verpelli, C., D'Avanzo, F., Tomanin, R., Vicidomini, C., Cajola, L., Manara, R., Sala, C., Scarpa, M., Vescovi, A.L., and De Filippis, L. (2016). Glial degeneration with oxidative damage drives neuronal demise in MPSII disease. *Cell Death Dis.* 7, e2331. <https://doi.org/10.1038/cddis.2016.231>.
- Zhang, S.C., Wernig, M., Duncan, I.D., Brustle, O., and Thomson, J.A. (2001). In vitro differentiation of transplantable neural precursors from human embryonic stem cells. *Nat. Biotechnol.* 19, 1129–1133. <https://doi.org/10.1038/nbt1201-1129>.